

Chapter 1

Fundamentals of Femtosecond Laser Modification of Bulk Dielectrics

Shane M. Eaton, Giulio Cerullo, and Roberto Osellame

Abstract Femtosecond laser pulses focused beneath the surface of a dielectric are absorbed through nonlinear photoionization mechanisms, giving rise to a permanent structural modification with dimensions on the order of a micrometer. At low pulse energies, the modification in many glasses is a smooth refractive index change, enabling photonic device fabrication. At higher pulse energies, the laser-induced modification may contain birefringent, periodic nanoplanes which align themselves orthogonally to the laser polarization. These nanogratings are not ideal for most waveguide devices but when the sample is exposed to hydrofluoric acid after writing, preferential chemical etching along the direction of the nanoplanes forms several millimeter-long buried microchannels which are useful for microfluidic applications. At even higher pulse energies, ultrahigh pressures within the focal volume lead to microexplosions causing empty voids which can be used for three-dimensional photonic bandgap devices and memories. In addition to pulse energy, other parameters have been shown to strongly influence the resulting morphology after femtosecond laser exposure including repetition rate, scan speed, focusing condition, polarization, pulse duration, depth, and direction.

1.1 Introduction

In 1996, Hirao's group showed that by focusing subpicosecond pulses in the bulk of transparent glass, the modification induced beneath the sample surface could be tailored to produce a permanent refractive index increase [1]. Because of the nonlinear nature of the interaction, absorption is confined to the focal volume inside

S.M. Eaton (✉) · G. Cerullo · R. Osellame

Istituto di Fotonica e Nanotecnologie - Consiglio Nazionale delle Ricerche (IFN-CNR), and
Department of Physics - Politecnico di Milano, Piazza Leonardo da Vinci 32, 20133, Milan, Italy
e-mail: shane.eaton@ifn.cnr.it; giulio.cerullo@fisi.polimi.it; roberto.osellame@ifn.cnr.it

the bulk material. By scanning the sample relative to the laser focus with computer-controlled motion stages, a region of increased refractive index could be formed along an arbitrary three-dimensional path, unlike traditional photolithography, which is limited to fabricating devices in-plane. In this chapter, the current understanding of the femtosecond laser–material interaction physics in the bulk of dielectrics is discussed and the important exposure conditions influencing the resulting waveguide properties are reviewed.

1.2 Femtosecond Laser–Material Interaction

Peak intensities on the order of 10 TW/cm^2 can be readily produced by focused femtosecond laser pulses from today’s commercial laser systems. Such intensities result in strong nonlinear absorption, allowing for localized energy deposition in the bulk of glasses. After several picoseconds, the laser-excited electrons transfer their energy to the lattice, leading to a permanent material modification. While a complete physical model of the laser–material interaction has thus far eluded researchers, the process can be simplified by subdivision into three main steps: the initial generation of a free electron plasma followed by energy relaxation and modification of the material.

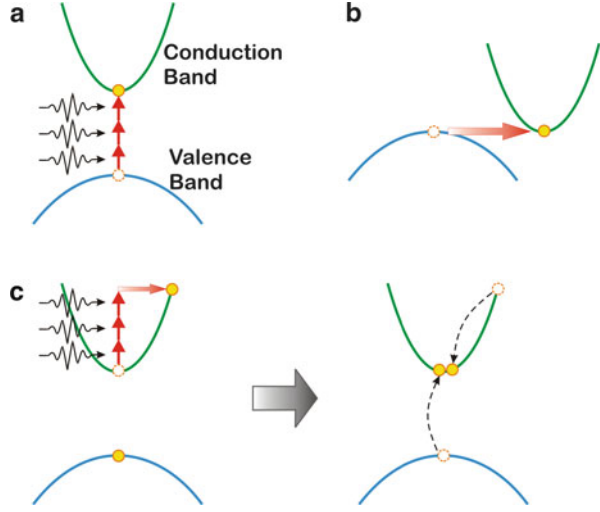
1.2.1 Free Electron Plasma Formation

Focused femtosecond laser pulses, with wavelengths in the visible or near-infrared spectra, have insufficient photon energy to be linearly absorbed in glasses. Valence electrons are instead promoted to the conduction band through nonlinear photoionization, which proceeds by multiphoton ionization and/or tunneling photoionization pathways depending on the laser frequency and intensity [2, 3]. If nonlinear photoionization were the only absorption process, the threshold intensity for optical breakdown would vary greatly with bandgap due to the large variation in absorption probability with bandgap (multiphoton absorption order). However, avalanche photoionization is also present and since it depends only linearly on laser intensity, there is only a small variation in optical breakdown threshold intensity with material bandgap energy [4]. Because of this low dependence of the breakdown threshold on the bandgap energy, femtosecond laser microfabrication can be applied in a wide range of materials.

1.2.1.1 Nonlinear Photoionization

Multiphoton absorption occurs due to the simultaneous absorption of multiple photons by an electron in the valence band (Fig. 1.1a). The number of photons m

Fig. 1.1 Nonlinear photoionization processes underlying femtosecond laser machining. **(a)** Multiphoton ionization, **(b)** tunneling ionization, and **(c)** Avalanche ionization: free carrier absorption followed by impact ionization [5]



required to bridge the bandgap must satisfy $mh\nu > E_g$, where E_g is the bandgap, and ν is the frequency of light. Multiphoton ionization is the dominant mechanism at low laser intensities and high frequencies (but below that which is needed for single photon absorption). At high laser intensity and low frequency, nonlinear ionization proceeds via tunneling, as shown in Fig. 1.1b. The strong field distorts the band structure and reduces the potential barrier between the valence and conduction bands. Direct band to band transitions may then proceed by quantum tunneling of the electron from the valence to conduction band. As shown by Keldysh [6], multiphoton and tunneling photoionization can be described in the same theoretical framework. The transition between the processes is described by the Keldysh parameter:

$$\gamma = \frac{\omega}{e} \sqrt{\frac{m_e c n \epsilon_0 E_g}{I}} \quad (1.1)$$

where ω is the laser frequency, I is the laser intensity at the focus, m_e is the effective electron mass, e is the fundamental electron charge, c is the speed of light, n is the linear refractive index and ϵ_0 is the permittivity of free space. If γ is much less (greater) than 1.5, tunneling (multiphoton) ionization dominates. For $\gamma \sim 1.5$, photoionization is a combination of tunneling and multiphoton ionization. For waveguide fabrication in dielectrics, typical laser, and material properties result in $\gamma \sim 1$, so that nonlinear ionization is a combination of both processes [3].

1.2.1.2 Avalanche Photoionization

Electrons present in the conduction band may also absorb laser light by free carrier absorption (Fig. 1.1c). After sequential linear absorption of several photons, a conduction band electron's energy may exceed the conduction band minimum by more than the band gap energy and the hot electron can then impact ionize a bound electron in the valence band, resulting in two excited electrons at the conduction band minimum. These two electrons can undergo free carrier absorption and impact ionization and the process can repeat itself as long as the laser field is present and strong enough, giving rise to an electron avalanche.

Avalanche ionization requires that sufficient seed electrons are initially present in the conduction band. These seed electrons may be provided by thermally excited impurity or defect states, or direct multiphoton or tunneling ionization. For subpicosecond laser pulses, absorption occurs on a faster time scale than energy transfer to the lattice, decoupling the absorption and lattice heating processes [3]. Seeded by nonlinear photoionization, the density of electrons in the conduction band grows through avalanche ionization until the plasma frequency approaches the laser frequency, at which point the plasma becomes strongly absorbing. For 1- μm wavelength laser radiation, the plasma frequency equals the laser frequency when the carrier density is on the order of 10^{21} cm^{-3} , which is known as the critical density of free electrons. At this high carrier density, only a few percent of the incident light is reflected by the plasma, so that most of the energy is transmitted into the plasma where it can be absorbed through free carrier absorption [3]. It is usually assumed that optical breakdown occurs when the number of carriers reaches this critical value. In glass, the corresponding intensity required to achieve optical breakdown is 10^{13} W/cm^2 .

Since the lattice heating time is on the order of 10 ps, the absorbed laser energy is transferred to the lattice long after the laser pulse is gone. Because short pulses need less energy to achieve the intensity for breakdown and because the absorption is decoupled from the lattice heating, more precise machining is possible relative to longer pulses. Further, because nonlinear photoionization can seed electron avalanche with femtosecond laser pulses, this results in deterministic breakdown. This is in contrast to the stochastic breakdown with longer pulses which rely on the low concentration of impurities (~ 1 impurity electron in conduction band per focal volume) randomly distributed in the material to seed an electron avalanche [7]. Lenzner et al. found that for very short pulses ($< 10 \text{ fs}$ and 100 fs in fused silica and borosilicate glasses, respectively), photoionization can dominate avalanche ionization and produce sufficient plasma density to cause damage by itself [8]. Schaffer et al. showed that the contribution from avalanche ionization is greater at longer pulse durations and for materials with greater band gap energies such as fused silica and sapphire [3].

1.2.2 Relaxation and Modification

It is well accepted that nonlinear photoionization and avalanche ionization from absorbed femtosecond laser pulses are responsible for the creation of a free electron plasma. However, once the electrons have transferred their energy to the lattice, the physical mechanisms for material modification are not fully understood. Of the hundreds of published works citing the pioneering work by Davis et al. [1], the observed morphological changes can be generally classified into three types of structural changes: a smooth refractive index change [9], a form birefringent refractive index modification [10–12], and microexplosions leading to empty voids [13]. The regime of modification and resulting morphological change depends not only on many exposure parameters (energy, pulse duration, repetition rate, wavelength, polarization, focal length, scan speed, and others) but also on material properties (bandgap, thermal conductivity, and others). However, in pure fused silica which is the most commonly processed material for waveguide writing, these three morphologies can be observed by simply changing the incident laser energy [14] as illustrated in Fig. 1.2. These morphologies are discussed below with emphasis on fused silica glass; further insight, also related to other glasses, will be provided in Chaps. 2, 3 and 4, while discussion on the main modification mechanisms in crystals and polymers can be found in Chaps. 11 and 12, respectively.

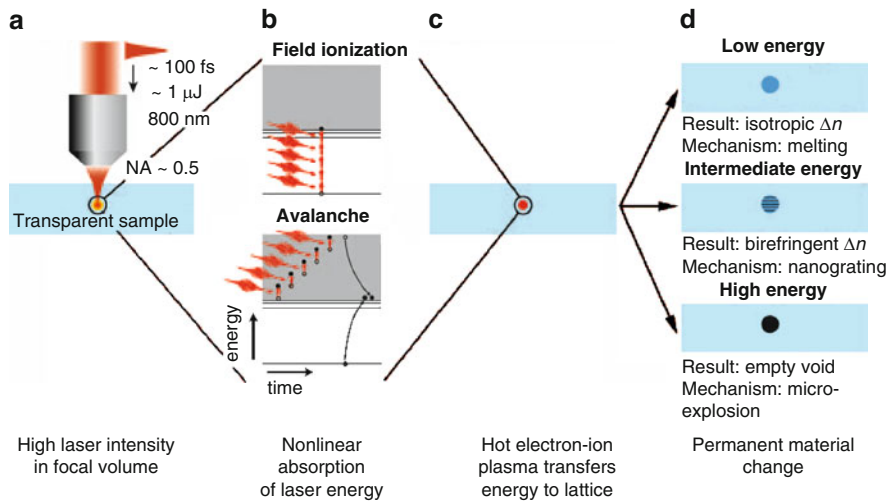


Fig. 1.2 Illustration of the interaction physics of focused femtosecond laser pulses in bulk fused silica. (a) The laser is focused below the sample surface resulting in a high intensity in the focal volume. (b) The energy is nonlinearly absorbed and a free electron plasma is created by multiphoton/tunneling and avalanche photoionization. (c) The plasma transfers its energy to the lattice on a ~ 10 ps time scale resulting in one of three types of permanent modification (d): isotropic refractive index change at low pulse energy, sub-wavelength birefringent nanostructures at moderate energy and empty voids at high pulse energy [14]

1.2.2.1 Smooth Refractive Index Change

An isotropic regime of modification is useful for optical waveguides, where smooth and uniform refractive index modification is required for low propagation loss. At low pulse energies just above the modification threshold (~ 100 nJ for 0.6-NA focusing of 800-nm, 100-fs pulses), a smooth refractive index modification has been observed in fused silica, which is attributed to densification from rapid quenching of the melted glass in the focal volume [15]. In fused silica, the density (refractive index) increases when glass is rapidly cooled from a higher temperature [16]. Micro-Raman spectroscopy has confirmed an increase in the concentration of 3 and 4 member rings in the silica structure in the laser exposed region, indicating a densification of the glass [15]. Shock waves generated by focused femtosecond laser pulses giving rise to stress have been shown to play a role in causing densification under certain conditions [17].

It has been argued that laser-induced color centers may be responsible for the laser-induced refractive index change through a Kramers–Kronig mechanism (a change in absorption leads to a change in refractive index) [18]. Although induced color centers have been observed in glasses exposed to femtosecond laser radiation [19, 20], to date there has been no experimental evidence of a strong link between color center formation and the induced refractive index change. Waveguides formed in fused silica with an infrared femtosecond laser [21] were found to exhibit photo-induced absorption peaks at 213 nm and 260 nm corresponding to SiE' (positively charged oxygen vacancies) and non-bridging oxygen hole centers (NBOHC) defects, respectively. However, both color centers were completely erased after annealing at 400°C , although waveguide behavior was still observed up to 900°C . Therefore, it is unlikely that color centers played a significant role in the refractive index change [21]. Other research found that the thermal stability of color centers produced in borosilicate and fused silica glasses by femtosecond laser irradiation is not consistent with that of the induced refractive index change [20]. Recently, Withford's group has shown for Yb-doped phosphate glasses used in waveguide lasers, femtosecond laser-induced color centers contribute approximately 15% to the observed refractive index increase [22]. Using integrated waveguide Bragg gratings, the authors were able to accurately study the photobleaching and thermal annealing of the induced color centers. The color centers were stable for temperatures below 70°C , which is below the operating point during lasing. However, the green luminescence generated by the Yb ions results in a photobleaching of the color centers during laser operation, resulting in reduced lifetime which must be corrected by pre-aging techniques [22].

Although a complete understanding of the femtosecond laser material interaction in forming optical waveguides has presently eluded researchers, it is certain that densification and color centers play a role. However, their contributions will vary depending on the glass composition and the femtosecond laser exposure conditions, further adding to the complexities in modeling femtosecond laser waveguide writing. In glasses with structures that are more complex than fused silica, further contributions must be considered. For example, in multicomponent crown glass, the

authors concluded that the ring-shaped refractive index profile during femtosecond laser irradiation was the result of ion exchange between network formers and network modifiers [23].

1.2.2.2 Birefringent Refractive Index Change

For higher pulse energies (~ 150 – 500 nJ for 0.6-NA focusing of 800-nm, 100-fs pulses), birefringent refractive index changes have been observed in the bulk of fused silica glass, as first reported by Sudrie et al. [10]. Kazansaky et al. argued that the birefringence was due to periodic nanostructures that were caused by interference of the laser field and the induced electron plasma wave [11]. In similarly exposed fused silica samples, Taylor's group observed periodic layers of alternating refractive index with sub-wavelength period that were clearly visualized after etching the laser-written tracks with HF acid (Fig. 1.3a and b). The orientation of the nanogratings was perpendicular to the writing laser polarization in all cases. The period of the nanostructures was found to be approximately $\lambda/2n$, regardless of scan speed, which implies a self-replicating formation mechanism [24]. However, new research suggests a slight variation of the nanograting period with exposure parameters [25]. Taylor's group proposed that inhomogeneous dielectric breakdown results in the formation of a nanoplasma resulting in the growth and self-organization of nanoplanes [24]. The model was found to accurately predict the experimentally measured nanograting period, but further development is needed to explain why nanostructures have not been observed in borosilicate glasses, and why they only form in a small window of pulse energy and pulse duration in fused silica [24]. Preferential HF etching of laser-written tracks was observed when the nanogratings were parallel to the writing direction (polarization perpendicular to scan direction) allowing the HF acid to diffuse more easily in the track, as shown in Fig. 1.3c. This effect can be exploited to fabricate buried microchannels for microfluidic applications [24, 26–28], which are discussed in detail in Chaps. 14 and 16.

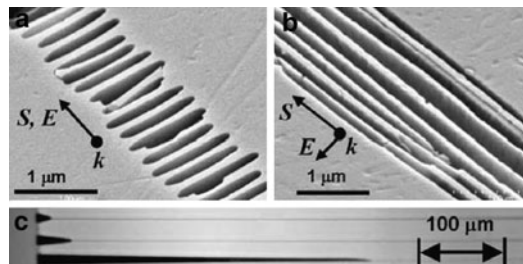
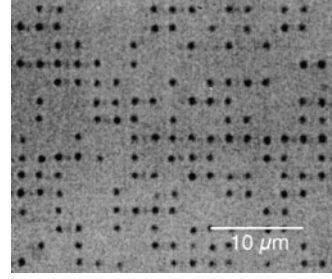


Fig. 1.3 Scanned electron microscope image of nanogratings formed at 65- μm depth (sample cleaved and polished at writing depth) with polarization parallel (a) and perpendicular (b) to the scan direction. Overhead view (c) of etched microchannels demonstrating polarization selective etching with parallel (top), 45° (middle) and perpendicular (bottom) linear polarizations [24]

Fig. 1.4 Binary bits (voids) recorded in fused silica with 100-fs laser [29]



1.2.2.3 Void Formation

At high pulse energies (>500 nJ for 0.6-NA focusing of 800-nm, 100-fs pulses) giving peak intensities greater than $\sim 10^{14}$ W/cm², pressures greater than Young's modulus are generated in the focal volume, creating a shockwave after the electrons have transferred their energy to the ions (~ 10 ps). The shockwave leaves behind a less dense or hollow core (void), depending on the laser and material properties [13]. By conservation of mass, this core is surrounded by a shell of higher refractive index. Such voids may be exploited for 3D memory storage [29] (Fig. 1.4) or photonic bandgap materials [30], but are not suitable for optical waveguides.

1.2.2.4 Multiple Pulse Interaction

The above interpretations for the structural changes induced by focused femtosecond lasers were based on single pulse interactions, but can likely be extended to explain modification from multiple pulses within the same laser spot, assuming the repetition rate is low enough that thermal diffusion has carried the heat away from the focus before the next pulse arrives [14]. In this situation, the ensuing pulses may add to the overall modification, but still act independently of one another.

For high-repetition rates (>100 kHz), the time between laser pulses is less than the time for heat to diffuse away, resulting in an accumulation of heat in the focal volume. If the pulse energy is sufficient, the glass near the focus is melted and as more laser pulses are absorbed, this melted volume increases in size until the laser is removed, at which point and the melt rapidly cools into a structure with altered refractive index. For a scanned waveguide structure, the size of the melted volume can be controlled by the effective number of pulses in the laser spot size, $N = 2w_0 R / v$, where $2w_0$ is the spot size diameter ($1/e^2$), R is the repetition rate and v is the scan speed. For cumulative heating, the morphology of the structural change is dominated by the heating, melting, and cooling dynamics of the material in and around the focal volume [14]. Laser repetition rate, along with other exposure variables in femtosecond laser waveguide writing are discussed in more detail in the following section.

1.3 Exposure Variables and Considerations

Below we review the important exposure parameters in femtosecond laser processing, with an emphasis on glass substrates. The important experimental variables in processing crystals and polymers are discussed in Chaps. 11 and 12, respectively.

1.3.1 Focusing

Linear optical effects such as dispersion, diffraction, aberration, and nonlinear effects such as self focusing, plasma defocusing, and energy depletion influence the propagation of focused femtosecond laser pulses in dielectrics, thereby altering the energy distribution at the focus and the resulting refractive index modification.

1.3.1.1 Linear Propagation

Incident femtosecond laser pulses are focused with an external lens to achieve a small micrometer-sized focal spot and drive nonlinear absorption. Neglecting spherical aberration and nonlinear effects, the spatial intensity profile of a femtosecond laser beam can be well represented by the paraxial wave equation and Gaussian optics. The diffraction-limited minimum waist radius w_0 (1/2 the spot size) for a collimated Gaussian beam focused in a dielectric is given by:

$$w_0 = \frac{M^2 \lambda}{\pi \text{NA}} \quad (1.2)$$

where M^2 is the Gaussian beam propagation factor (beam quality) [31], NA is the numerical aperture of the focusing objective and λ is the free space wavelength. The Rayleigh range z_0 (1/2 the depth of focus) inside a transparent material of refractive index n is given by:

$$z_0 = \frac{M^2 n \lambda}{\pi \text{NA}^2} \quad (1.3)$$

Chromatic and spherical aberration cause a deviation in the intensity distribution near the focus such that (1.2), and (1.3) may no longer be valid approximations. Chromatic aberration as the result of dispersion in the lens is corrected by employing chromatic aberration-corrected microscope objectives for the wavelength spectrum of interest. For lenses made with easily-formed spherical shapes, light rays which are parallel to the optic axis but at different distances from the optic axis fail to converge to the same point, resulting in spherical aberration. This issue can be addressed by using multiple lenses such as those found in microscope objectives, or employing an aspheric focusing lens. In waveguide writing where light is focused inside glass, the index mismatch at the air-glass interface introduces

additional spherical aberration. As a result, there is a strong depth dependence for femtosecond-laser written buried structures [32–34]. This depth dependence is more pronounced for higher NA objectives [3], except in the case of oil-immersion lenses [3,35,36] or dry objectives with collars that enable spherical aberration correction at different focusing depths [33]. Other solutions to the problem of spherical aberration are described in Chaps. 4 and 5.

Dispersion from mirror reflection and transmission through materials can broaden the pulse width [37] which can reduce the peak intensity and alter the energy dissipation at the focus. For a typical Yb-based amplified femtosecond laser with 1- μm wavelength and 10-nm bandwidth, the dispersion in glass is -50 ps/km/nm and the pulse duration increase per length is 5 fs/cm. Since these sources have pulse durations >200 fs, the dispersion is negligible for most laser micromachining beam delivery systems which have less than 1 cm of transmission through glass. It is only for short pulse <40-fs oscillators with large bandwidths that dispersion becomes an issue. In this case, pre-compensation of the dispersion through the microscope objective is required to obtain the shortest pulse at the focus [37].

1.3.1.2 Nonlinear Propagation

When light propagates through a dielectric material, it induces microscopic displacement of bound charges, forming oscillating electric dipoles that add up to the macroscopic polarization. In amorphous glass which has an inversion center ($\chi^{(2)} = 0$), the polarization vector is given by:

$$\mathbf{P} = \epsilon_0 \left[\chi^{(1)} + \frac{3}{4} \chi^{(3)} |\mathbf{E}|^2 \right] \mathbf{E} \quad (1.4)$$

where \mathbf{E} is the electric field vector and $\chi^{(i)}$ is the i -th order susceptibility, with 4th and higher orders left out of (7.5) due to negligible contribution. The refractive index can be identified from (7.5) as:

$$n = \sqrt{1 + \chi^{(1)} + \frac{3}{4} \chi^{(3)} |\mathbf{E}|^2} = n_0 + n_2 I \quad (1.5)$$

where $n_0 = \sqrt{1 + \chi^{(1)}}$ is the linear refractive index, $n_2 = 3\chi^{(3)}/4\epsilon_0 c n_0^2$ is the nonlinear refractive index and $I = \frac{1}{2} \epsilon_0 n_0 c |\mathbf{E}|^2$ is the laser intensity.

The spatially varying intensity of a Gaussian laser beam can create a spatially varying refractive index in dielectrics. Because n_2 is positive in most materials, the refractive index is higher at the center of the beam compared to the wings. This variation in refractive index acts as a positive lens and focuses the beam inside a dielectric with a strength dependent on the peak power. If the peak power of the femtosecond laser pulses exceeds the critical power for self-focusing [3]:

$$P_c = \frac{3.77\lambda^2}{8\pi n_0 n_2} \quad (1.6)$$

the collapse of the pulse to a focal point is predicted. However, as the beam self focuses, the increased intensity is sufficient to nonlinearly ionize the material to produce a free electron plasma, which acts as a diverging lens that counters the Kerr lens self-focusing. A balance between self focusing and plasma defocusing leads to filamentary propagation, which results in axially elongated refractive index structures, which are undesirable for transversely written waveguide structures described in the next section. Self-focusing can be suppressed in waveguide fabrication by tightly focusing the laser beam with a microscope objective to reach the intensity for optical breakdown without exceeding the critical power for self focusing.

In fused silica, $n_0 = 1.45$ and $n_2 = 3.5 \times 10^{-20} \text{ m}^2/\text{W}$ [38] so that for $\lambda = 800 \text{ nm}$, the critical power is $\sim 1.8 \text{ MW}$. From (1.6), the critical power is proportional to the square of the laser wavelength; therefore, lower critical powers result when working with the second and third harmonic frequencies of femtosecond lasers. Also, the critical power is inversely related to the nonlinear (and linear) refractive index, presenting a challenge in forming waveguides in nonlinear materials such as heavy metal oxide ($n_0 \sim 2$, $n_2 \sim 10^{-18} \text{ m}^2/\text{W}$ [39]) and chalcogenide glasses ($n_0 \sim 2.5$, $n_2 \sim 10^{-17} \text{ m}^2/\text{W}$ [40]), polymers ($n_0 \sim 1.5$, $n_2 \sim 10^{-18} \text{ m}^2/\text{W}$), lithium niobate ($n_0 \sim 2.3$, $n_2 \sim 10^{-19} \text{ m}^2/\text{W}$ [41]) and silicon ($n_0 \sim 3.5$, $n_2 \sim 10^{-18} \text{ m}^2/\text{W}$ [42]) crystals.

1.3.2 Writing Geometry

The standard configurations for laser-writing of optical waveguides are shown in Fig. 1.5. In longitudinal writing, the sample is scanned parallel, either toward or away from the incident laser. In this configuration, the resulting waveguide structures have cylindrical symmetry, owing to the transverse symmetry Gaussian intensity profile of the laser beam. The main disadvantage of the longitudinal writing geometry is that the waveguide length is limited by the working distance of the lens, which for a typical focusing objective with $\text{NA} = 0.4$, is approximately 5 mm. To overcome this issue, researchers have employed looser focusing lenses ($\text{NA} \sim 0.2$) [43], requiring higher laser power to reach the intensity required for optical breakdown. At such peak powers ($\sim 1 \text{ MW}$), the optical Kerr effect results in self focusing, producing filaments which yield refractive index change structures elongated in the axial direction by up to several hundred microns [43]. Despite the long length of the filaments, fabrication speeds are still relatively slow at $\sim 1 \mu\text{m/s}$ to build up enough refractive index increase to efficiently guide light [43].

In the transverse writing scheme of Fig. 1.5, the sample is scanned orthogonally relative to the incoming laser. The working distance no longer restricts the

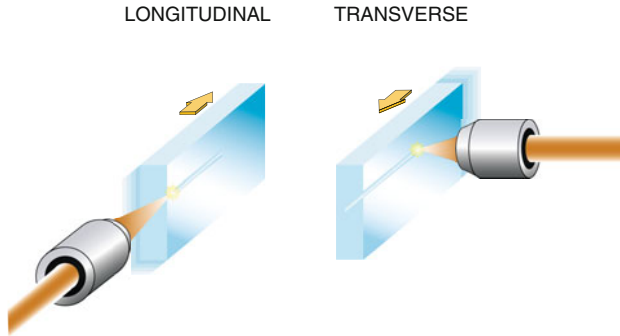


Fig. 1.5 Longitudinal and transverse writing geometries for femtosecond laser waveguide fabrication in the bulk of transparent materials. In transverse (longitudinal) writing, the sample is scanned transverse (parallel) with respect to the incident femtosecond laser [4]

waveguide's length and structures may be formed over a depth range of several millimeters, which is sufficient flexibility for many applications to provide 3D optical circuits. The disadvantage of the transverse geometry is that the waveguide cross section is asymmetric due to the ratio between depth of focus and spot size $2z_0/2w_0 = n/\text{NA}$, where n is the refractive index and NA is the numerical aperture. Since waveguides are formed in glasses with $n = 1.5$ with typical NA of 0.25 to 0.85, the focal volume asymmetry n/NA varies from 6.0 to 1.8. This asymmetry results in elliptical waveguide cross sections with elliptical guided modes, which couple poorly to optical fibers. To overcome this focal volume asymmetry, special beam shaping methods are required as described in Chap. 5.

1.3.3 Influence of Exposure Variables Within Low- and High-Repetition Rate Regimes

The advent of high-repetition rate femtosecond lasers is opening new avenues for manipulating thermal relaxation effects [34–36, 44–46] that control the properties of optical waveguides formed when the ultrashort pulse lasers are focused inside dielectrics. As repetition rate increases, the time between laser pulses becomes shorter than the time for the absorbed laser radiation to diffuse out of the focal volume and heat builds up around the focal volume. This effect was first exploited in the surface micromachining of glass to form smooth, crack-free holes due to laser interaction with a thin sheath of ductile pre-heated glass [47]. Schaffer et al. reported a dramatic increase in the size of laser-modified structures formed in the bulk of glass under strong heat accumulation effects with a 25-MHz laser oscillator over structures formed by diffusion-only processes [44]. The combination of high-repetition rate and heat accumulation offers fast writing speeds and cylindrically symmetric waveguides together with benefits of annealing and decreased thermal

cycling that are associated with low propagation and coupling loss to standard optical fiber [45]. Detailed discussion on the resulting waveguide characteristics within low (1–100 kHz) and high (>100 kHz) repetition rate regimes as a function of scan speed and pulse energy can be found in Chap. 7.

In addition to pulse energy, scan speed, and focusing, several other exposure parameters have been found to influence the resulting properties of femtosecond laser-written waveguides. These factors include pulse duration [48, 49], polarization [10, 50], direction [51], wavelength [52], spatiotemporal beam shaping, and waveguide cross section engineering (i.e., slit focusing, astigmatic focusing, and multiscan writing) [53, 54]. The effect of these parameters are briefly described below but in detail in the subsequent chapters.

Waveguides formed in fused silica with moderate fluence show no evidence of heat accumulation even as the repetition rate is raised from 1 kHz [50] to 1 MHz [34] and the waveguide properties were found to be strongly dependent on the incident writing polarization. In contrast, no detectable difference in insertion loss or mode size was found when waveguides were formed with different polarizations in borosilicate glass within the heat accumulation regime at MHz repetition rates [34]. In addition, the waveguide properties in borosilicate glass were invariant to pulse duration when varied from 300 to 700 fs, which is in contrast to results in fused silica, where pulse duration was observed to strongly affect waveguide mode size and loss [50]. The sensitivity to pulse duration and polarization in fused silica is associated with form birefringence arising from nanogratings formed within the laser-modified volume [12]. In borosilicate glass, nanogratings have not been observed [24], and such polarization and pulse duration dependence may possibly be erased by the strong thermal annealing [24] within the heat accumulation regime.

Due to energy depletion, self focusing and plasma defocusing, pulse duration strongly also influences the spatial distribution of the energy density in the focal volume [55, 56]. At 1-kHz repetition rate, where heat accumulation is not present, the dependence of waveguide properties on pulse duration in lithium niobate [56] and fused silica glass [57] was attributed to nonlinear pulse propagation. However, in the heat accumulation regime, nearly spherically symmetric thermal diffusion washes out the elliptical distribution of energy in the focal volume to yield waveguides with cross sections that are relatively circular. Therefore, one would expect pulse duration, despite its effect on the energy distribution at the focus, to play a lesser role on the properties of waveguides fabricated in the heat accumulation regime.

Kazansky et al. recently discovered the quill effect [51], in which laser material modification is influenced by the writing direction, even in amorphous glass with a symmetric laser intensity distribution. The researchers conclusively showed that the cause of the directional writing dependence is due to a pulse front tilt in the ultrafast laser beam [51]. Although any material should show a direction dependence due to a pulse front tilt, the effect was found to be almost negligible when processing borosilicate glass within the heat accumulation regime as evidenced by a directional coupler formed by arms written in opposite direction but showing a remarkably high peak coupling ratio of 99%, [58]. Further details of the quill effect are provided in Chap. 6.

As described in Chap. 7, wavelength is an important variable when processing high bandgap materials such as pure fused silica. Due to its large bandgap and low melting point, the increased fluence and lower order of multiphoton absorption provided by the second harmonic wavelength enabled stronger index contrast and lower loss waveguides in this material [52]. An infrared wavelength of $1.5\ \mu\text{m}$ was applied to fused silica [21], revealing a very wide energy processing window of 1 to $23\ \mu\text{J}$ in forming smooth waveguides compared to 0.5 to $2.0\ \mu\text{J}$ at 800-nm wavelength. Such a large processing window is desirable, but the added complexity of using an optical parametric amplifier has dissuaded researchers from adopting this approach for waveguide device fabrication. By tuning the wavelength of a standard 800-nm Ti:Sapphire amplifier to the mid infrared ($2.4\ \mu\text{m}$), linear absorption was avoided in silicon, making it possible to form buried waveguides in silicon via a 3-photon multiphoton absorption process [42].

To correct for asymmetric waveguide cross sections produced by low repetition rate fabrication as described above, several solutions have been proposed including astigmatic focusing [59] and slit focusing [60], deformable mirror beam reshaping [61] and multiscan writing [53]. More details on these techniques can be found in Chap. 5. The effects of varying the spatial and temporal properties of a laser beam for improving waveguide formation are discussed in Chap. 4.

1.4 Summary

It was shown that femtosecond laser pulses focused beneath the surface of a dielectric are initially absorbed through nonlinear and avalanche photoionization. After energy relaxation, the material is permanently modified within the small laser focal volume. If the laser pulse energy is just above the optical breakdown threshold, the modification can be tailored to be a smooth refractive index change, which is useful for optical waveguide devices. In addition to pulse energy, the waveguide properties depend on many other exposure variables, but principally on repetition rate, which determines whether the modification regime is due to individual pulses or cumulative pulse heating. The subsequent chapters will give more insight into the interaction of femtosecond laser pulses with glasses, crystalline, and polymer materials and highlight the many exciting devices created by the femtosecond laser micromachining method.

References

1. K. Davis, K. Miura, N. Sugimoto, K. Hirao, *Opt. Lett.* **21**(21), 1729 (1996)
2. B.C. Stuart, M.D. Feit, S. Herman, A.M. Rubenchik, B.W. Shore, M.D. Perry, *Phys. Rev. B* **53**(4), 1749 (1996)
3. C. Schaffer, A. Brodeur, E. Mazur, *Meas. Sci. Technol.* **12**(11), 1784 (2001)

4. R.R. Gattass, E. Mazur, *Nat. Photon.* **2**(4), 219 (2008)
5. M. Ams, G.D. Marshall, P. Dekker, M. Dubov, V.K. Mezentsev, I. Bennion, M.J. Withford, *IEEE J. Sel. Top. Quantum Electron.* **14**(5), 1370 (2008)
6. L.V. Keldysh, *Sov. Phys. JETP* **20**(5), 1307 (1965)
7. D. Du, X. Liu, G. Korn, J. Squier, G. Mourou, *Appl. Phys. Lett.* **64**(23), 3071 (1994)
8. M. Lenzner, J. Krger, S. Sartania, Z. Cheng, C. Spielmann, G. Mourou, W. Kautek, F. Krausz, *Phys. Rev. Lett.* **80**(18), 4076 (1998)
9. K. Miura, J.R. Qiu, H. Inouye, T. Mitsuyu, K. Hirao, *Appl. Phys. Lett.* **71**(23), 3329 (1997)
10. L. Sudrie, M. Franco, B. Prade, A. Mysyrowicz, *Opt. Commun.* **171**(4-6), 279 (1999)
11. Y. Shimotsuma, P.G. Kazansky, J. Qiu, K. Hirao, *Phys. Rev. Lett.* **91**(24), 247405 (2003)
12. C. Hnatovsky, R.S. Taylor, P.P. Rajeev, E. Simova, V.R. Bhardwaj, D.M. Rayner, P.B. Corkum, *Appl. Phys. Lett.* **87**(1) (2005). 014104
13. S. Juodkazis, K. Nishimura, S. Tanaka, H. Misawa, E.G. Gamaly, B. Luther-Davies, L. Hallo, P. Nicolai, V.T. Tikhonchuk, *Phys. Rev. Lett.* **96**(16), 166101 (2006)
14. K. Itoh, W. Watanabe, S. Nolte, C.B. Schaffer, *MRS Bull.* **31**(8), 620 (2006)
15. J. Chan, T. Huser, S. Risbud, D. Krol, *Opt. Lett.* **26**(21), 1726 (2001)
16. R. Bruckner, *J. Non-Cryst. Solids* **5**(2), 123 (1970)
17. M. Sakakura, M. Shimizu, Y. Shimotsuma, K. Miura, K. Hirao, *Appl. Phys. Lett.* **93**(23), 3 (2008)
18. K. Hirao, K. Miura, *J. Non-Cryst. Solids* **239**(1-3), 91 (1998)
19. J. Chan, T. Huser, S. Risbud, D. Krol, *Appl. Phys. A* **A76**(3), 367 (2003)
20. A. Streltsov, N. Borrelli, *J. Opt. Soc. Am. B* **19**(10), 2496 (2002)
21. A. Saliminia, R. Vallee, S.L. Chin, *Opt. Commun.* **256**(4-6), 422 (2005)
22. P. Dekker, M. Ams, G.D. Marshall, D.J. Little, M.J. Withford, *Opt. Exp.* **18**(4), 3274 (2010)
23. S. Kanehira, K. Miura, K. Hirao, *Appl. Phys. Lett.* **93**(2), 3 (2008)
24. C. Hnatovsky, R.S. Taylor, E. Simova, P.P. Rajeev, D.M. Rayner, V.R. Bhardwaj, P.B. Corkum, *Appl. Phys. A* **84**(1-2), 47 (2006)
25. L.P.R. Ramirez, M. Heinrich, S. Richter, F. Dreisow, R. Keil, A.V. Korovin, U. Peschel, S. Nolte, A. Tunnermann, in *Frontiers in Ultrafast Optics: Biomedical, Scientific, and Industrial Applications X*, vol. 7589 (SPIE, San Francisco, California, USA, 2010), vol. 7589, pp. 758,919-8
26. A. Marcinkevicius, S. Juodkazis, M. Watanabe, M. Miwa, S. Matsuo, H. Misawa, J. Nishii, *Opt. Lett.* **26** (2001)
27. Y. Bellouard, A. Said, M. Dugan, P. Bado, *Opt. Exp.* **12**(10), 2120 (2004)
28. V. Maselli, R. Osellame, G. Cerullo, R. Ramponi, P. Laporta, L. Magagnin, P.L. Cavallotti, *Appl. Phys. Lett.* **88**(19), 191107 (2006)
29. E. Glezer, M. Milosavljevic, L. Huang, R. Finlay, T.H. Her, T. Callan, E. Mazur, *Opt. Lett.* **21**(24), 2023 (1996)
30. S. Juodkazis, S. Matsuo, H. Misawa, V. Mizeikis, A. Marcinkevicius, H.B. Sun, Y. Tokuda, M. Takahashi, T. Yoko, J. Nishii, *Appl. Surf. Sci.* **197-198**, 705 (2002)
31. T.F. Johnston, *Appl. Opt.* **37**(21), 4840 (1998)
32. A. Marcinkevicius, V. Mizeikis, S. Juodkazis, S. Matsuo, H. Misawa, *Appl. Phys. A.* **76**(2), 257 (2003)
33. C. Hnatovsky, R.S. Taylor, E. Simova, V.R. Bhardwaj, D.M. Rayner, P.B. Corkum, *J. Appl. Phys.* **98**(1), 013517 (2005). 013517
34. S.M. Eaton, H. Zhang, M.L. Ng, J. Li, W.J. Chen, S. Ho, P.R. Herman, *Opt. Exp.* **16**(13), 9443 (2008)
35. R. Osellame, N. Chiodo, G. Della Valle, G. Cerullo, R. Ramponi, P. Laporta, A. Killi, U. Morgner, O. Svelto, *IEEE J. Sel. Top. Quantum Electron.* **12**(2), 277 (2006)
36. K. Minoshima, A. Kowalevich, I. Hartl, E. Ippen, J. Fujimoto, *Opt. Lett.* **26**(19), 1516 (2001)
37. R. Osellame, N. Chiodo, V. Maselli, A. Yin, M. Zavelani-Rossi, G. Cerullo, P. Laporta, L. Aiello, S. De Nicola, P. Ferraro, A. Finizio, G. Pierattini, *Opt. Exp.* **13**(2), 612 (2005)
38. L. Sudrie, A. Couairon, M. Franco, B. Lamouroux, B. Prade, S. Tzortzakis, A. Mysyrowicz, *Phys. Rev. Lett.* **89**(18) (2002). 186601

39. J. Siegel, J.M. Fernandez-Navarro, A. Garcia-Navarro, V. Diez-Blanco, O. Sanz, J. Solis, F. Vega, J. Armengol, *Appl. Phys. Lett.* **86**(12) (2005). 121109
40. V. Ta'eed, N.J. Baker, L. Fu, K. Finsterbusch, M.R.E. Lamont, D.J. Moss, H.C. Nguyen, B.J. Eggleton, D.Y. Choi, S. Madden, B. Luther-Davies, *Opt. Exp.* **15**(15), 9205 (2007)
41. J. Burghoff, C. Grebing, S. Nolte, A. Tuennermann, *Appl. Phys. Lett.* **89**(8) (2006). 081108
42. A.H. Nejadmalayeri, P.R. Herman, J. Burghoff, M. Will, S. Nolte, A. Tuennermann, *Opt. Lett.* **30**(9), 964 (2005)
43. K. Yamada, W. Watanabe, T. Toma, K. Itoh, J. Nishii, *Opt. Lett.* **26**(1), 19 (2001)
44. C. Schaffer, J. Garcia, E. Mazur, *Appl. Phys. A* **A76**(3), 351 (2003)
45. S.M. Eaton, H. Zhang, P.R. Herman, F. Yoshino, L. Shah, J. Bovatsek, A.Y. Arai, *Opt. Exp.* **13**(12), 4708 (2005)
46. R. Osellame, N. Chiodo, G. Valle, S. Taccheo, R. Ramponi, G. Cerullo, A. Killi, U. Morgner, M. Lederer, D. Kopf, *Opt. Lett.* **29**(16), 1900 (2004)
47. P. Herman, A. Oettl, K. Chen, R. Marjoribanks, in *Proceedings of the SPIE - The International Society for Optical Engineering*, vol. 3616 (SPIE, San Jose, CA, USA, 1999), vol. 3616, pp. 148–55
48. H. Zhang, S.M. Eaton, J. Li, A.H. Nejadmalayeri, P.R. Herman, *Opt. Exp.* **15**(7), 4182 (2007)
49. T. Fukuda, S. Ishikawa, T. Fujii, K. Sakuma, H. Hosoya, *Proceedings of the SPIE - The International Society for Optical Engineering* **5279** (2004)
50. D.J. Little, M. Ams, P. Dekker, G.D. Marshall, J.M. Dawes, M.J. Withford, *Opt. Exp.* **16**(24), 20029 (2008)
51. W. Yang, P.G. Kazansky, Y. Shimotsuna, M. Sakakura, K. Miura, K. Hirao, *Appl. Phys. Lett.* **93**(17), 171109 (2008)
52. L. Shah, A. Arai, S. Eaton, P. Herman, *Opt. Exp.* **13**(6), 1999 (2005)
53. Y. Nasu, M. Kohtoku, Y. Hibino, *Opt. Lett.* **30**(7), 723 (2005)
54. R.R. Thomson, H.T. Bookey, N.D. Psaila, A. Fender, S. Campbell, W.N. MacPherson, J.S. Barton, D.T. Reid, A.K. Kar, *Opt. Exp.* **15**(18), 11691 (2007)
55. D.M. Rayner, A. Naumov, P.B. Corkum, *Opt. Exp.* **13**(9), 3208 (2005)
56. J. Burghoff, H. Hartung, S. Nolte, A. Tuennermann, *Appl. Phys. A* **86**(2), 165 (2007)
57. H. Zhang, S.M. Eaton, P.R. Herman, *Opt. Exp.* **14**(11), 4826 (2006)
58. S.M. Eaton, W. Chen, H. Zhang, R. Iyer, M.L. Ng, S. Ho, J. Li, J.S. Aitchison, P.R. Herman, *IEEE J. Lightwave Technol.* **27**(9) (2009)
59. R. Osellame, S. Taccheo, M. Marangoni, R. Ramponi, P. Laporta, D. Polli, S. De Silvestri, G. Cerullo, *J. Opt. Soc. Am. B* **20**(7), 1559 (2003)
60. M. Ams, G.D. Marshall, D.J. Spence, M.J. Withford, *Opt. Exp.* **13**(15), 5676 (2005)
61. R.R. Thomson, A.S. Bockelt, E. Ramsay, S. Beecher, A.H. Greenaway, A.K. Kar, D.T. Reid, *Opt. Exp.* **16**(17), 12786 (2008)

Femtosecond Laser Micromachining
Photonic and Microfluidic Devices in Transparent
Materials

Osellame, R.; Cerullo, G.; Ramponi, R. (Eds.)

2012, XVIII, 486 p., Hardcover

ISBN: 978-3-642-23365-4